Supplementary Material: Cell-cell contacts limit public goods dispersal inside *P. aeruginosa* microcolonies

Thomas Julou[1†], Thierry Mora[1†], Laurent Guillon[4],Vincent Croquette[1], Isabelle J. Schalk[4], David Bensimon[1,3], Nicolas Desprat[1,2*]

[1]Laboratoire de Physique Statistique (UMR8550), École Normale Supérieure, 24, rue Lhomond, 75005 Paris, France

[2] Université Paris Diderot 75205 PARIS CEDEX 13

[3] Dept. of Chemistry and Biochemistry, UCLA, Los-Angeles

[4]Biotechnologie et signalisation cellulaire (UMR 7242), Université de Strasbourg-CNRS, ESBS, Blvd Sébastien Brant, F-67413 Illkirch, Strasbourg, France

[*]To whom correspondence should be addressed; desprat@ens.fr

[†] These two authors contributed equally

Correlation imaging Correlation images were reconstructed from a z-stack of microcolonies observed under bright field illumination. A z-stack is composed of a 32 frames taken by step of $200\mathrm{nm}$ below and above the focal plane of a microcolony. For each pixel, the experimental intensity profile in the vertical direction is correlated with a reference profile defined by the derivative of a gaussian: $-(z - z_0)\exp -\frac{(z-z_0)^2}{2\sigma^2}$, where z_0 is the position of the focus in the stack and σ corresponds to the typical size of a bacteria ($700\mathrm{nm}$). The result of the correlation sets then the intensity of the pixel for the new correlation image.

From cell segmentation performed on correlation images, we obtained the individual mask for all the bacteria in the microcolony. If a pixel is outside all individual mask, it is then defined

as a background pixel. To measure the fluorescence in each cell, we subtracted the average fluorescence of the background to the fluorescence measured on each mask. The concentration c is then given as the sum of the fluorescence over the pixels of the cell normalized by the area of the cell.

To calibrate the intracellular pyoverdine concentration, we spin-coated samples containing a known concentration of pyoverdine in polyvinyl alcohol and measured the intensity of fluorescence. In this study, an average intensity of 1000 arbitrary units for a cell corresponds to ~ 500 molecules of pyoverdine.

Exchange model. For the $\Delta fpvA$ strain, there is no uptake $k_{\rm in} = 0$ and no positive feedback $f = 0$. Hence, we expect $\lambda^{\Delta fpvA} = k_{\rm out} + \nu > \nu$ and $\kappa^{\Delta fpvA} = 0$. For the $\Delta pvdRT/Q$ strain, which secretes less pyoverdine, $k_{\rm out}^{\Delta pvdRT/Q} < k_{\rm out}^{WT}$. Hence, we expect $\lambda^{\Delta pvdRT/Q} < \lambda^{WT}$.

Mean colony behaviour. The dynamics of the mean pyoverdine concentration in the microcolonies is obtained by averaging Eq. (1) of the main text over cells, yielding

$$d\bar{c}/dt = \alpha - \gamma\bar{c}, \tag{1}$$

with $\gamma = \lambda - \kappa$, and where noise self-averages to zero. The bar $\bar{c}$ denotes the colony mean. The solution to this equation is

$$\bar{c}(t) = \frac{\alpha}{\gamma}\left[1 - e^{-\gamma t}\right]$$

The observed linear dependence of $\bar{c}(t)$ with t indicates that $\gamma < 1/(400\ \mathrm{min})$ (the total time of an experiment). To better estimate γ, we fitted the data for $d\bar{c}/dt$ to a line: $d\bar{c}/dt \approx \alpha[1 - \gamma t]$, which gave $\gamma \approx 10^{-3}\ \mathrm{min}^{-1}$.

Parameter estimation. In order to estimate the remaining parameters of the model (κ and the noise), we used a mean-field approximation, which amounts to treating the average pyoverdine

concentration from the cell's neighbors c_{neigh}, as if it were the colony average. We thus write:

$$dc_{\mathrm{neigh}}/dt = \alpha - \gamma c_{\mathrm{neigh}}$$

as in Eq. (1). Subtracting this expression from Eq. (1) of the main text, we get

$$dc'/dt = -\lambda c' + \mathrm{noise}$$

where $c' = c - c_{\mathrm{neigh}}$ is proportional to the fluorescence contrast between one cell and its neighbors. The equation for c' describes the dynamics of an Ornstein-Uhlenbeck process. To estimate λ, we binned the data points according to their value of c' (each point in a bin is then the fluorescence contrast of one cell at one time). For each bin, we estimated dc'/dt by perfoming a linear fit of $c'(t+\delta t) - c'(t)$ *versus* δt, for δt ranging from 3 to 15 min. The result of this fit is displayed as a function of c' in Fig. 2A. A linear fit of dc'/dt against c' yields λ. The error on λ is the standard deviation obtained by repeating the procedure on the 10 experiments. We also checked that the value of λ did not depend on the absolute concentration c, by further binning data according to c, and repeating the procedure for each c-bin (Fig. S4).

We next computed the noise term: $\mathrm{noise}(t) = dc'/dt + \lambda c'$. While λ did not depend on c it turns out that the noise depends strongly on the mean concentration of siderophores in the colony. Consequently we binned the noise data according to the fluorescence level (siderophore concentration c) and for each c-bin we looked at the temporal autocorrelation function

$$C_{\mathrm{noise}}(t) = \langle \mathrm{noise}(t_0) \cdot \mathrm{noise}(t_0 + t) \rangle$$

see Fig. 2B. Here $\langle \ldots \rangle$ denotes an ensemble average, *i.e.* an average over realisations of the noise and should not be confused with the colony mean (e.g. $\bar{c}$). Each curve was fitted to an exponential: $C_{\mathrm{noise}}(t) = \hat{A} e^{-|t|/\tau}$. Since $\tau \sim 10$ min is smaller than all other typical times (e.g. λ^{-1} or the mean time between divisions ν^{-1}), we approximated this exponential by a Dirac delta-function. The magnitude of the noise is then equal to the integral of the autocorrelation

function: $\int_{-\infty}^{\infty} C_{\rm noise}(t)dt = 2\hat{A}\tau$. As seen from the inset in Fig. 2B, the noise level depends quadratically on the average fluorescence (pyoverdine concentration at time t_0) in the colony:

$$\langle \text{noise}(t_0) \cdot \text{noise}(t_0 + t) \rangle = 2\hat{A}\tau\delta(t) = 2\Gamma\bar{c}(t_0)^2\delta(t). \tag{2}$$

As a check, we repeated the analysis on the normalised concentration $x = c/\bar{c}$, whose dynamics is given in the adiabatic approximation ($(1/c)dc/dt \ll \lambda$) by $dx/dt = -\lambda x + \xi(t)$, with $\xi(t) = \text{noise}/\bar{c}$. The adiabatic approximation was tested in all colonies and on average: $\langle (1/c)dc/dt \rangle \sim 10^{-3}\,\text{min}^{-1}$. To validate the dynamical equation for the normalized variable x, we verified that the noise term $\xi(t)$ was independent of the normalization c. We binned the data according to c and for each c-bin fitted the correlation function to an exponential:

$$C_\xi(t) = \langle \xi(t_0 + t)\xi(t_0) \rangle = A_0 e^{-|t|/\tau}$$

We found that the properties of the normalized noise $C_\xi(t)$ were independent of c (Fig. S8, hence $\hat{A} = A_0\bar{c}(t_0)^2$), in particular its magnitude $\Gamma = A_0\tau$ is constant (inset). Thus we computed the mean value of Γ by averaging the values obtained from the data for each experiment (Fig. S9).

An Ornstein-Uhlenbeck process can be solved analytically to give the statistics of fluctuations at steady state: $\langle c' \rangle = 0$ and $\langle c'^2(t) \rangle = \Gamma\bar{c}^2/\lambda$. This prediction is compared to the experiments in Fig. 2B. All variances and standard deviation were estimated from data using an unbiased estimator with a $1/(N-1)$ normalization factor, where N is the sample size [1].

Spatial model. The mean concentration in the immediate neighborhood of a cell i can be written as: $c_{i,\text{neigh}} = (1/n_i)\sum_{j \text{ neigh of } i} c_j$, where n_i is the number of neighbors of cell i's . Then we have:

$$dc_i/dt = \alpha + \kappa\left(\frac{1}{n_i}\sum_{j \text{ neigh of } i} c_j - c_i\right) - \gamma c_i + \text{noise} \equiv \alpha + \kappa[\Delta c]_i - \gamma c_i + \text{noise}. \tag{3}$$

which is a diffusion equation (with leakage) on the lattice formed by cell adjacency. Δ is the lattice equivalent of the Laplace operator. Within the adiabatic approximation $(1/c)(dc/dt) \ll \lambda$ (see above), we can write a similar equation for x:

$$dx_i/dt = \tilde{\alpha} + \kappa[\Delta x]_i - \tilde{\gamma} x_i + \xi(t), \tag{4}$$

where $\xi(t)$ is defined as before, $\tilde{\alpha} = \alpha/\bar{c}$, and $\tilde{\gamma} = \gamma + (1/\bar{c})d\bar{c}/dt$.

To predict the average pyoverdine distribution in a colony, we calculated the steady state $\langle x_i \rangle$ for each snapshot of a colony, by solving for $d\langle x_i \rangle/dt = 0$ (*i.e.* Eq. (4) without the noise term) while fixing the average value of $\langle x_i \rangle$ at the colony edge (< 1 μm) from its measured value. $\tilde{\alpha}$ is left as a free parameter enforcing $\bar{x} = 1$. The adjacency network was obtained by a Voronoi tessellation of the cell centers. Δ was calculated from this adjacency network and then symmetrized. To plot Fig. 2C, the average values $\langle x_i \rangle$ thus obtained were binned according to their distance to the colony edge. The average value of the relative contrast $\langle x'_i \rangle \equiv [\Delta \langle x \rangle]_i$ is shown as a function of the distance to the edge in Fig. S5. The temporal autocorrelations of the fluctuations of x_i and $x'_i = (\Delta x)_i$ are given by:

$$\langle \delta x(t_0) \delta x(t_0 + t) \rangle = \Gamma \sum_a e^{-(\gamma + \kappa \mu_a)t}/(\gamma + \kappa \mu_a) \tag{5}$$

and

$$\langle \delta x'(t_0) \delta x'(t) \rangle = \Gamma \sum_a \mu_a^2 e^{-(\gamma + \kappa \mu_a)t}/(\gamma + \kappa \mu_a), \tag{6}$$

where μ_a are the eigenvalues of Δ. The temporal correlations of the local fluctuations x'_i are compared to the data in Fig. 2D. The spatial correlations of the fluctuations were calculated using

$$\langle \delta x_i(t) \delta x_j(t) \rangle = \Gamma \sum_{a,b} U_{ia} [\gamma + \kappa(\mu_a + \mu_b)/2]^{-1} U_{bj} \tag{7}$$

and

$$\langle \delta x'_i(t) \delta x'_j(t) \rangle = \Gamma \sum_{a,b} [\Delta U]_{ia} [\gamma + \kappa(\mu_a + \mu_b)/2]^{-1} [U \Delta]_{bj}, \tag{8}$$

where U is the matrix of eigenvectors of Δ. The total spatial correlation function represented in Fig. S6, $(\langle x_i - 1)(x_j - 1)\rangle$, was calculated as the sum of the spatial heterogeneities, $\overline{(\langle x_i\rangle - 1)(\langle x_j\rangle - 1)}$,and local fluctuations: $\langle \delta x_i(t)\delta x_j(t)\rangle$. Similarly, the theoretical distribution in the inset of Fig. 1D inset was estimated by adding Gaussian fluctuations of variance $\langle \delta x_i(t)\delta x_j(t)\rangle$ to the distribution of the calculated $\langle x_i\rangle$. Fluctuations from the local background $\langle \delta x'_i(t)\delta x'_j(t)\rangle$ are compared to data in Fig. S7.

History of Pvd concentration in the neighboring cells According to the exchange model, [PFe] is proportional to the concentration $c_{\rm neigh}$ of free Pvd in the neighbouring cells. The evolution of internal iron is given by uptake and dilution from cell division, where $\nu = \log(2)/(\text{division time})$ is the growth rate:

$$d[\mathrm{Fe}]_{\rm int}/dt = \kappa[\mathrm{PFe}] - \nu[\mathrm{Fe}]_{\rm int} \tag{9}$$

Solving this equation yields $[\mathrm{Fe}]_{\rm int}(t) = \int_{-\infty}^{t} \kappa c_{\rm neigh}(t')exp[-\nu(t-t')]dt'$. This quantity is called c_n in the main text.

Simulation of spatial competition for mixed population. As observed in the experiments, 10% of synthesized pyoverdine diffuses freely. In cells, pyoverdine evolution is given by Eq. (1) of the main text, where $c_{\rm neigh}$ was taken as the average in the four nearest neighbors. External iron was either made to diffuse homogeneously and rapidly across the population (consisently with the high diffusion constant of $\mathrm{Fe}^{2+} = 7.6 \cdot 10^{-6}$ cm^2/sec in water [2]) or alternatively was assumed not to diffuse at all. Iron uptake was proportional to the concentration of the pyoverdine-iron complex, $[\mathrm{PFe}]$, calculated from the following equations:

- $[\mathrm{P}][\mathrm{Fe}]/[\mathrm{PFe}] = K_d^* = 500$ nM, where $K_d^* = 2[\mathrm{Tsf}]K_d(\mathrm{Pvd})/K_d(\mathrm{Tsf})$ is an effective dissociation constant calculated by assuming that all iron not complexed with pyoverdine is complexed with transferrin, which has two binding sites for iron ($[\mathrm{Tsf}] = 5\,\mu$M,

$K_d(\mathrm{Pvd}) = 0.5\ 10^{-24}$M [3] and $K_d(\mathrm{Tsf}) = 10^{-23}$M [4])

- $[\mathrm{PFe}] + [\mathrm{P}] = c_{\mathrm{out}} \sim c_{\mathrm{neigh}} + c$, equivalent to setting $a = b = 1$. In the simulation we set, a=1, b=0, *i.e.* $c_{\mathrm{out}} = c_{\mathrm{cneigh}}$ corresponds to the worst-case scenario for producers, as cells only benefit from their neighbors' production, and not directly from their own. Setting a=b=1, which might be more realistic, would give a further advantage of producers over non-producers.

- $[\mathrm{Fe}] + [\mathrm{PFe}] = [\mathrm{Fe}]_{\mathrm{tot}} = 2.5\,\mu\mathrm{M}$ [3].

The evolution of internal iron is given by Eq. 9. The pyoverdine production rate α was chosen so that the average pyoverdine concentration in a monoclonal population of producers is $\sim 2\,\mu\mathrm{M}$ (estimated from our data). $\gamma = \lambda - \kappa$ was set to 0.03ν. Notice that since we want to simulate long-term evolution, we need to assume that pyoverdine concentration reaches steady state, which is why we assign a non-zero value to γ. The relative fitness f of each cell was calculated from the internal iron concentration as:

$$f = 2[\mathrm{Fe}]_{\mathrm{int}}/([\mathrm{Fe}]_{\mathrm{int}} + [\mathrm{Fe}]^{(0)}_{\mathrm{int}}) - C, \tag{10}$$

where $[\mathrm{Fe}]^{(0)}_{\mathrm{int}}$ is the wild type value (*i.e.* obtained from a monoclonal population of producers at steady-state), and C is the production cost (zero for non-producers and a tunable parameter for producers). The particular form of iron-dependence of the fitness was chosen so that:

(*a*) it is zero when $[\mathrm{Fe}]_{\mathrm{int}} = 0$

(b) it saturates at large $[\mathrm{Fe}]$.

(*c*) as observed in the experiment (Fig 5.C): an 10% increase in $[\mathrm{Fe}]_{\mathrm{int}}$ results in a 5% increase in growth rate. So, its relative dependency upon $[\mathrm{Fe}]_{\mathrm{int}}$ around $[\mathrm{Fe}]^{(0)}_{\mathrm{int}}$ is 50%, which set the exponent n of the general Hill function ($f = 2[\mathrm{Fe}]^{\mathrm{n}}_{\mathrm{int}}/([\mathrm{Fe}]^{\mathrm{n}}_{\mathrm{int}} + ([\mathrm{Fe}]^{(0)}_{\mathrm{int}})^{\mathrm{n}}) - C$) equal to 1.

The fitness is here defined so that the expected number of offsprings after time $\log(2)/\nu$ is 2^f, where ν is the wild type (producer) growth rate in a monoclonal colony at steady state, without the production cost. Consistenly, when $[\mathrm{Fe}]_{\mathrm{int}} = [\mathrm{Fe}]_{\mathrm{int}}^{(0)}$ and there is no cost ($C = 0$), $f = 1$ and the expected number of offsprings is 2.

A continuous and uniform flux of external iron was injected at each point so that the amount of iron in all forms remains constant at $2.5\,\mu\mathrm{M}$. Competition was modeled as follows. At each generation and for each cell, we pick a random neighbor among the four nearest to compete with. The cell was replaced by its neighbor with probability $\max[0, (2^{f_{\mathrm{neigh}}} - 2^f)/(2^{f_{\mathrm{neigh}}} + 2^f)]$, where f is the fitness of the cell of interest, and f_{neigh} the fitness of its neighbor. We simulated the competition for 4,000 generations, starting with a population made of 50% non-producers and 50% producers randomly distributed on the lattice.

Estimation of the production cost from the literature. Since the number of offspring in our simulation, (*i.e* the growth rate, is given by the fitness defined in Eq. (10), the ratio $\frac{\Delta\nu}{\nu_{\mathrm{wt}}} = \frac{\nu_{\mathrm{mut}} - \nu_{\mathrm{wt}}}{\nu_{\mathrm{wt}}}$ is a direct measurement of the relative cost of production that is depicted on the ordinate of the phase diagram (Fig. 4). Although we measured the parameter λ/ν in our experiments, we cannot directly estimate the relative cost C of production because the benefits of ferri-pyoverdine uptake depends strongly on the spatial structure under the microscope. However, several studies have reported the outcome of competitions in liquid conditions between wild type strains (PAO1, natural isolates) and mutants that are defective for pyoverdine production (Δpvd, mutants derived from directed mutagenesis PAO6609, etc...) [5, 6, 7]. As in liquid conditions, every cells enjoys the same benefit, the ratio $\frac{\Delta\nu}{\nu_{\mathrm{wt}}} = C$ only accounts for the production cost and can be easily estimated from the plots. The data reported in the literature are expressed as $v = \frac{x_{\mathrm{mut}}(t_{\mathrm{end}})}{1-x_{\mathrm{mut}}(t_{\mathrm{end}})} \frac{1-x_{\mathrm{mut}}(0)}{x_{\mathrm{mut}}(0)}$ [5], $p = x_{wt}(t_{end})$ [6] or $W = \frac{\ln(x_{\mathrm{wt}}(t_{\mathrm{end}})/x_{\mathrm{wt}}(0))}{\ln(x_{\mathrm{mut}}(t_{\mathrm{end}})/x_{\mathrm{mut}}(0))}$ [7], where $x_{\mathrm{mut}}(t)$ and $x_{\mathrm{wt}}(t)$ are the frequency of mutants and wild type cells, respectively. These

observables are related to our relative production cost by the following equations : $C = \frac{\ln(v)}{\ln(2)N}$, $C = \frac{\ln[(\frac{1}{p}-1)\frac{x_{\mathrm{wt}}(0)}{x_{\mathrm{mut}}(0)}]}{\ln(2)N}$ and $C = \frac{1-W}{W}$ where N represents the number of generations elapsed from 0 to t_{end}. N is estimated from the density of cell inoculation, except for [6] where this number is given explicitly. In Table S2, we summarised the conditions of competitions and how the estimation of the relative production cost $C = \frac{\Delta\nu}{\nu_{\mathrm{wt}}}$ measured from data available in the literature.

***P. aeruginosa* strains**	**relevant characteristics**	**reference**
PAO1	wild type strain	[8]
PAO1*pvdRTopmQ*	derivative of PAO1; Δ*pvdRTopmQ*, chromosomally integrated	[9]
PAO1*fpvA*	derivative of PAO1; Δ*fpvA*, chromosomally integrated	[10]
PAO1*pvdA*	derivative of PAO1; Δ*pvdA*, chromosomally integrated	[11]
pvdA-yfp	derivative of PAO1; pvdA-eyfp, chromosomally integrated	[12]

Table S 1: Strain Table.

Strains	**Mix Ratio**	**Culture Medium**	**Competition Time**	**Measured Parameter**	**Production Cost**
average over pairs [5]	1:1	CAA + Pvd	24h	$v = 1.1$	$C = 2\%$
PAO1 vs PAO6609 [6]	1:1	CAA + 100$\mu g.mL^{-1}$Tsf	6x24h	$p = 0.34$	$C = 2.3\%$
PAO1 vs PAO6609 [7]	1:1	CAA + 100$mg.mL^{-1}$Tsf	72h	$W = 0.96$	$C = 4.2\%$

Table S 2: Estimation of the relative production cost $C = \frac{\Delta\nu}{\nu_{wt}}$ measured from the data available in the literature. In [5], the cost is estimated from Fig. 5A (Pvd type I) with N=7. In [6], the cost is estimated from Fig. 3 (global and low r) with N=42. In [7], the cost is estimated from Fig. 4 (2.5g of Casamino acids) with N=7.

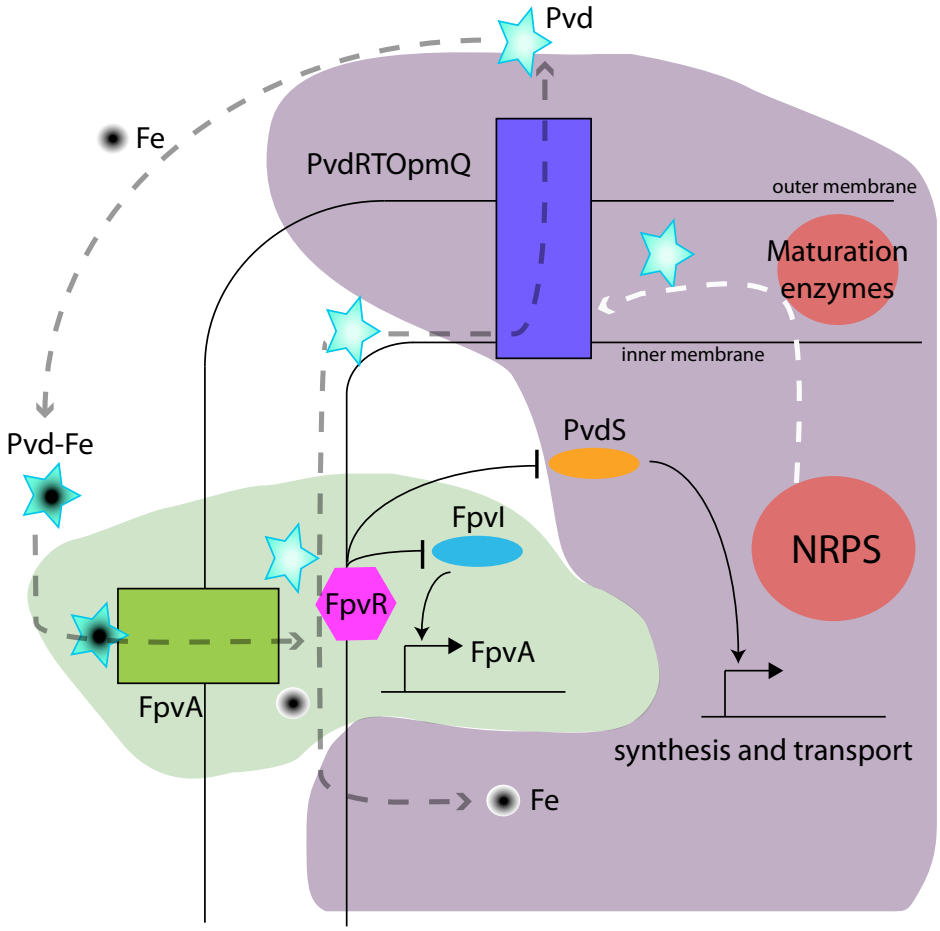

Fig. S 1: Diagram of Pvd pathway. Pyoverdine biosynthesis starts in the cytoplasm and ends in the periplasm. It involves four cytoplasmic non-ribosomal peptide synthetases (NRPS) and probably seven different other cytoplasmic and periplasmic enzymes [13, 14, 15]. Newly synthesized Pvd is stored in the bacterial periplasm [14] before secretion into the extracellular medium by the efflux system PvdRT-OpmQ [16]. After iron chelation in the extracellular medium, ferri-Pvd is transported across the outer membrane by the outer membrane transporter FpvA [17] and iron is released from the siderophore in *P. aeruginosa* periplasm [18]. Free-Pvd is then recycled into the extracellular medium by the efflux pump PvdRT-OpmQ [9, 19]. Pyoverdine biosynthesis is under a positive feedback regulated by two sigma factors PvdS and FpvI associated with their anti-sigma factor FpvR [20, 21]. When ferri-Pvd binds to FpvA, the outer membrane transporter interacts with FpvR. This interaction triggers the release of FpvI and PvdS that will activate the transcription of *fpvA* (light green) and all other genes involved in the pyoverdine pathway (light purple), respectively.

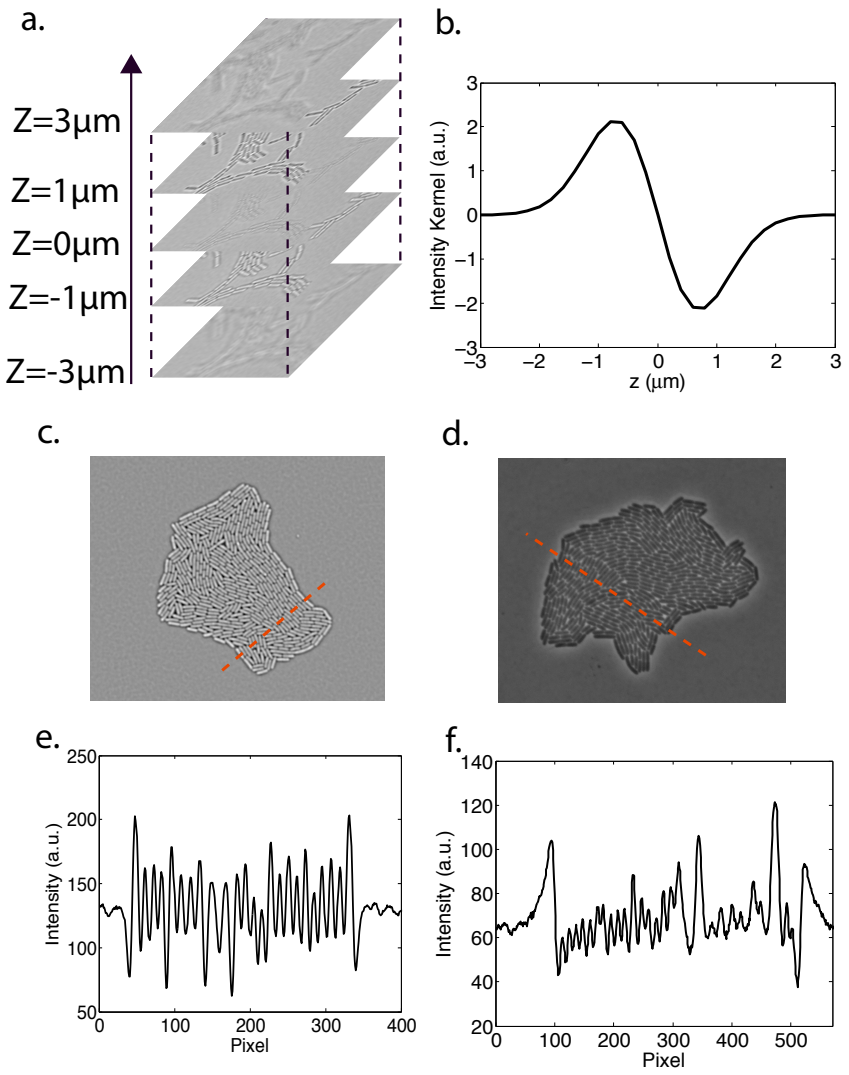

Fig. S 2: a) A z-stack of bright field images $I(x, y, z)$ are taken around the focal position. The vertical step is set at 200nm. The bacteria appear white when the z-position of the objective is below the focal plane and black when the z-position of the objective is above the focal plane (z=0). b) Each pixel of the observation field is correlated in the z-direction with an analytical kernel $Ker(z)$ that corresponds to the derivative of a gaussian function centered on the focal plane and with standard deviation $\sigma_z = 700$nm. c) Correlated image: $I_c(x, y, z = 0) = \int dz' I(x, y, z') Ker(z - z')$. d) Phase contrast image. Unlike phase-contrast images, the correlation images display regular fluctuations around the background level (compare (e) and (f)). In addition, the cell interior and membrane anticorrelate, enhancing the contrast of the images.

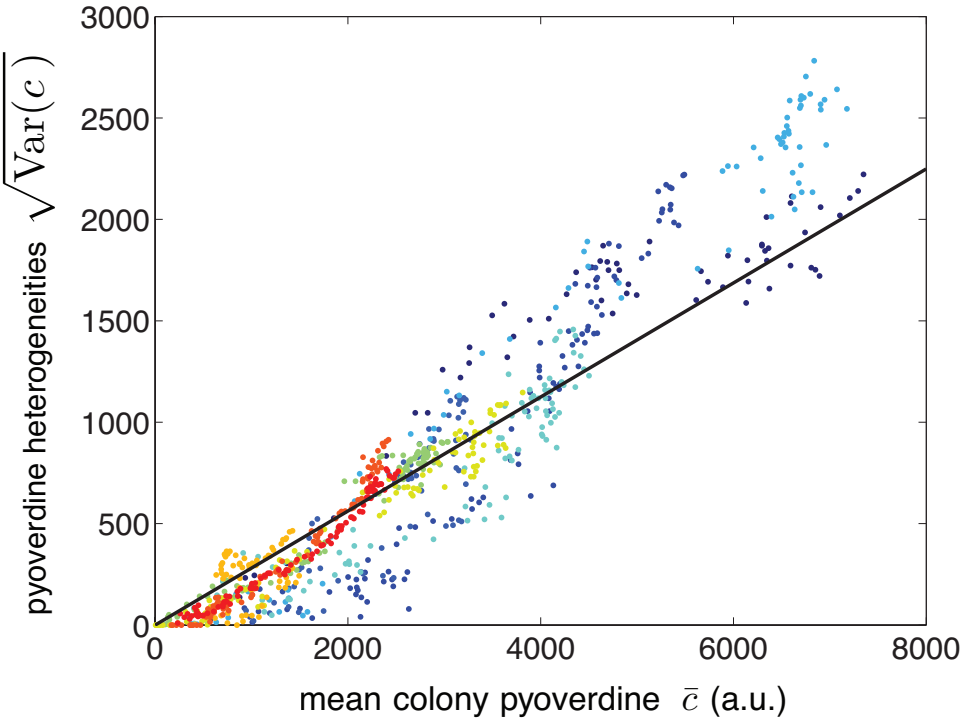

Fig. S 3: Standard deviation of heterogeneities in pyoverdine concentration c vs. mean pyoverdine concentration in colony $\bar{c}$. Black line is model prediction.

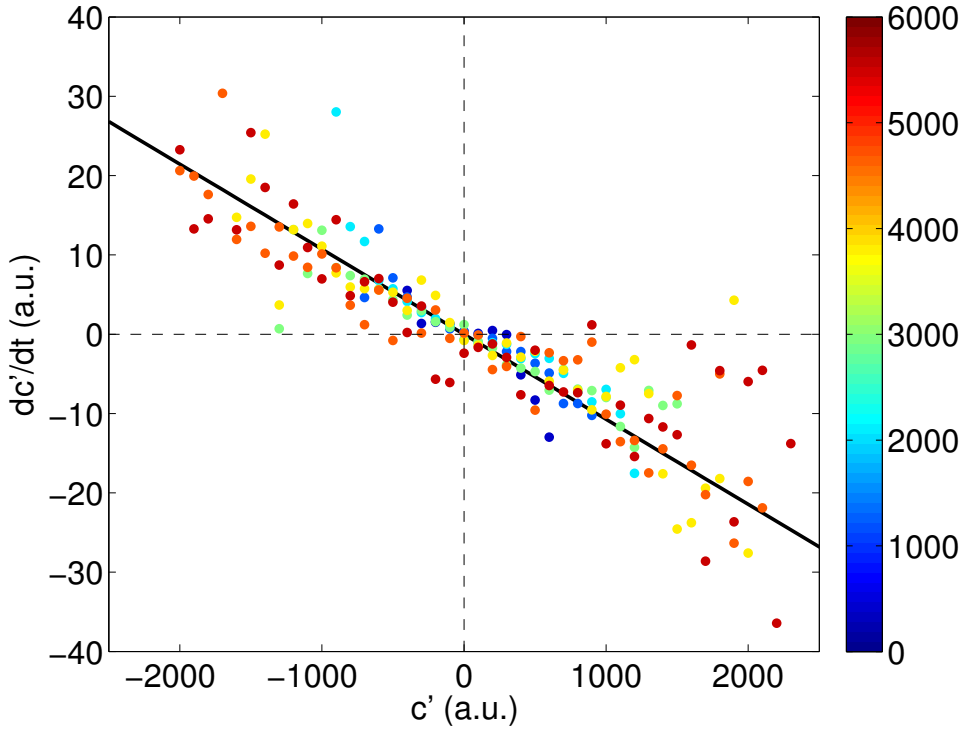

Fig. S 4: λ does not depend on absolute concentration. Same plot as Fig.2A in the main text, but here the data were pooled and color-coded according to the mean fluorescence (i.e. $\bar{c}$) in the colony. λ can also be fitted for each colony separately. The value $\lambda = 1.07 \pm 0.1 \cdot 10^{-2}$ min^{-1} reported in the main text and used in this plot (black line) is the average of this fit over different colonies.

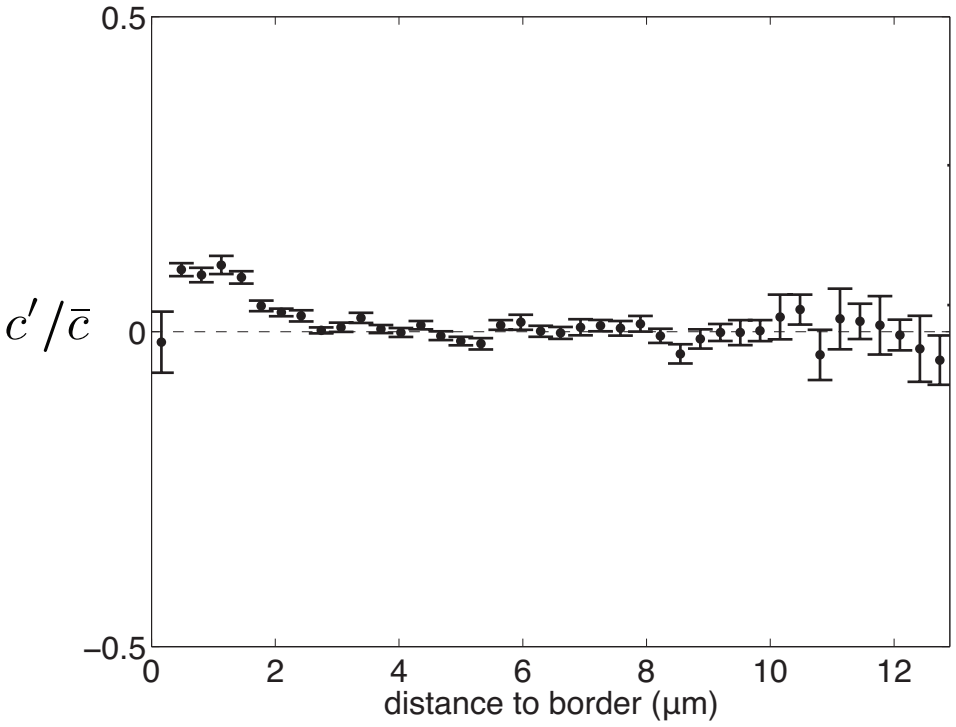

Fig. S 5: The normalised fluctuations $c'/\bar{c} = (c - c_{\mathrm{neigh}})/\bar{c}$ does not depend on the distance to the edge, except very close to it. Error bars represent SEM.

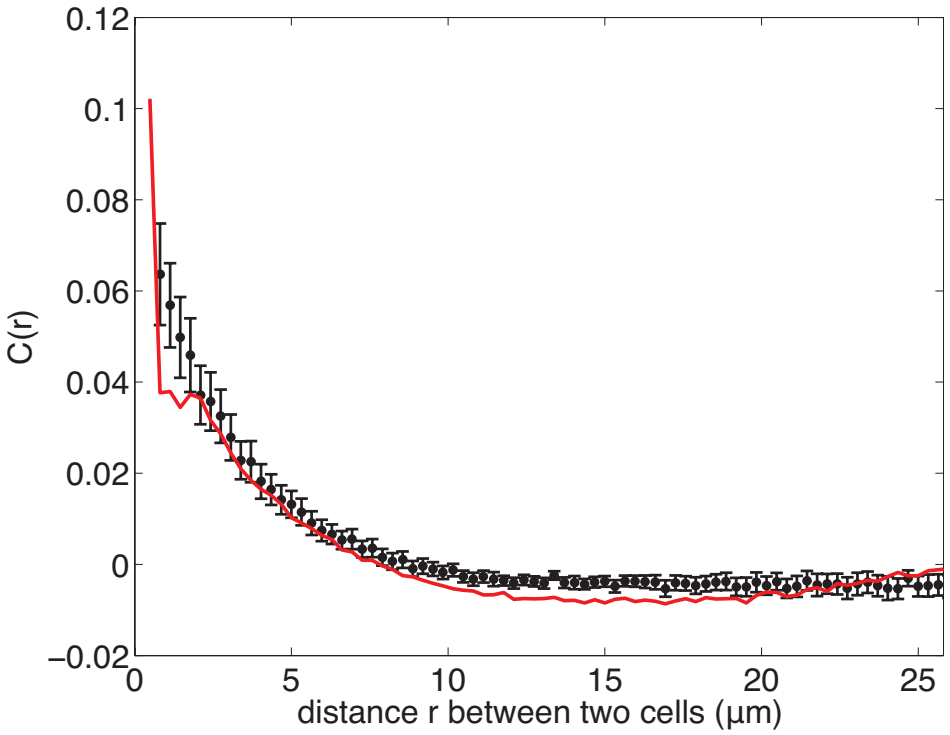

Fig. S 6: Spatial correlations of pyoverdine heterogeneities $C(r) = \sum_{ij} c_i c_j \delta(|\vec{r}_i - \vec{r}_j| - r) / \sum_{ij} \delta(|\vec{r}_i - \vec{r}_j| - r) - \bar{c}^2$. The prediction ot the model (red) is obtained as the sum of two contributions: (*i*) the correlation functions of local fluctuations; (*ii*) the concentration heterogeneities due to boundary effects and obtained by solving the diffusion equation for a mean pyoverdine concentration set by the cells on the edge of the colony. Error bars represent SEM.

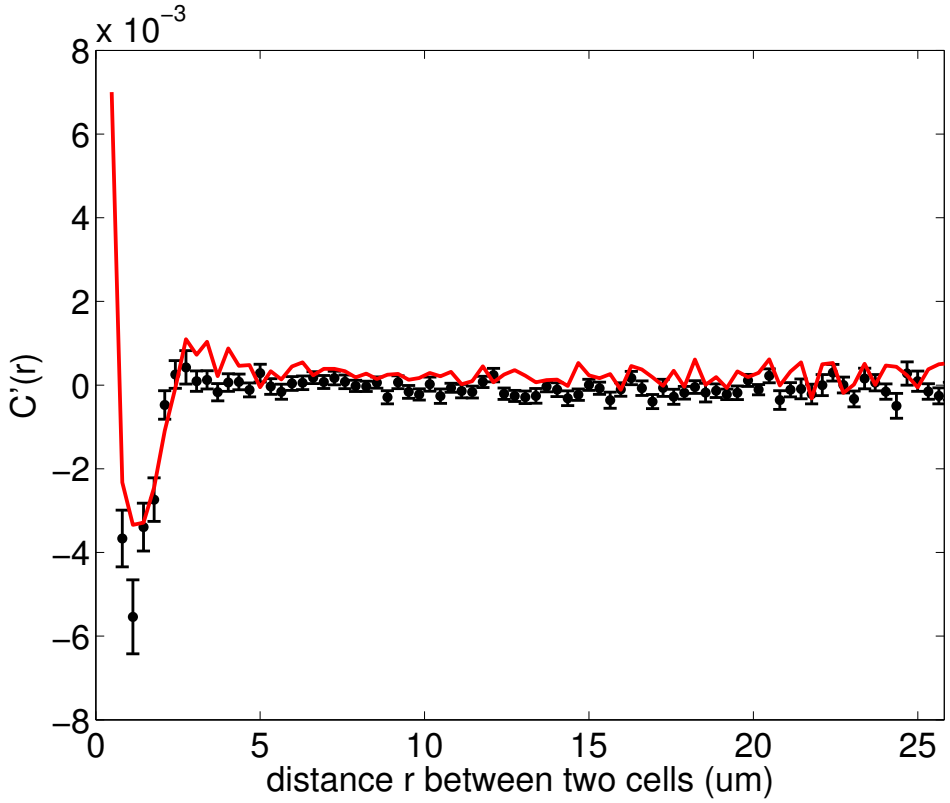

Fig. S 7: Same as Fig. S6, with $c' = c - c_{\mathrm{neigh}}$ instead of c. Fluctuation correlations are local. The negative lobe is an artifact of the fact that when i and j are neighbors, c_j contributes to $c_{i,\mathrm{neigh}}$, and vice-versa, resulting in a negative correlation. Error bars represent SEM.

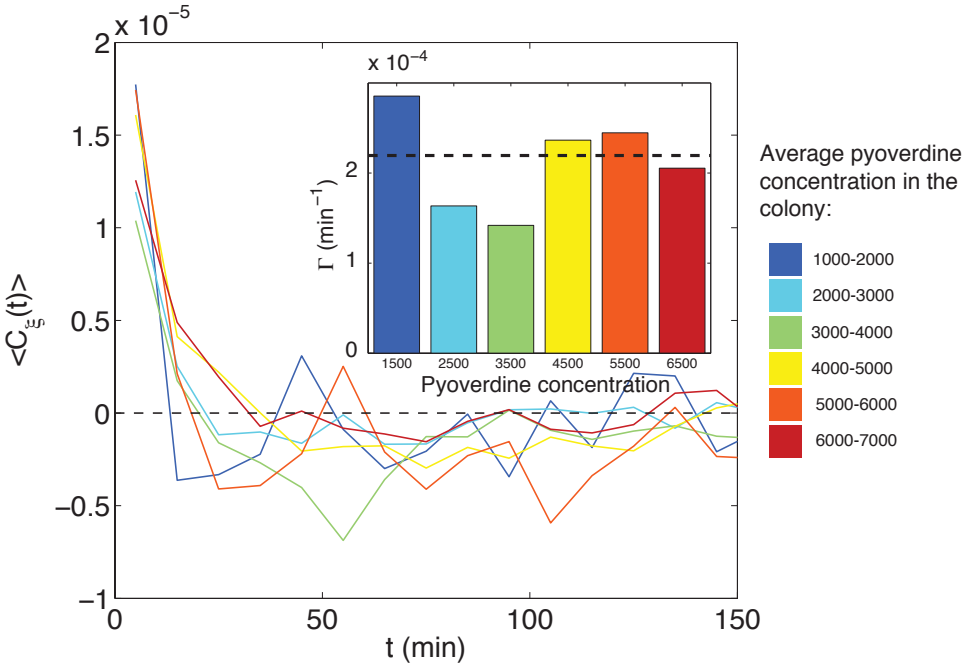

Fig. S 8: Same as Fig. 2B, but considering the normalised noise $\xi(t) = \mathrm{noise}(t)/\bar{c}$. Temporal autocorrelation function of the normalized noise: $C_\xi(t) = \langle \xi(t)\xi(t_0+t)\rangle - \langle \xi(t)\rangle\langle \xi(t_0+t)\rangle$, for various values of the mean pyoverdine concentration in the colony, $\bar{c}$. As before, this function can be approximated by $Ae^{-t/\tau}$, which we fit for each pyoverdine level. We approximate $C_\xi(t) = 2\Gamma\delta(t)$, with $\Gamma = A\tau$. Inset: Γ shows no systematic dependence on $\bar{c}$. Dashed line: average Γ calculated from all 10 colonies (Fig. S9).

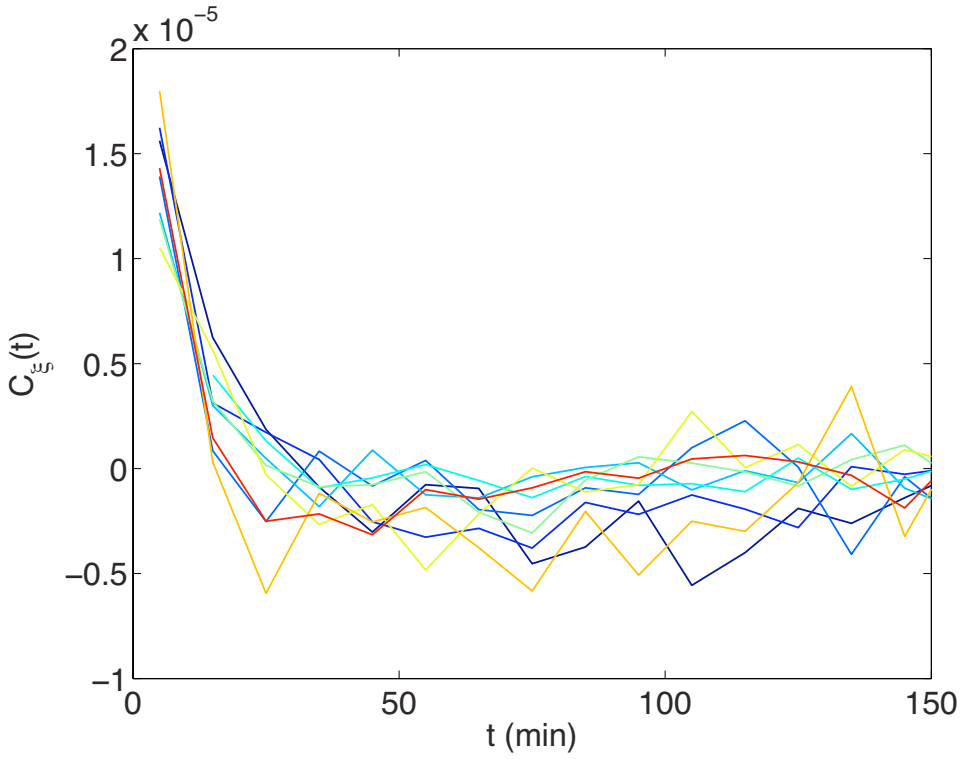

Fig. S 9: Same as Fig. S8, but plotted for each colony. For each plot, Γ is calculated from an exponential fit as before. The value $\Gamma = 2.19 \pm 0.17 \cdot 10^{-4}$ min^{-1} reported in the main text is an average over the plots for the different colonies.

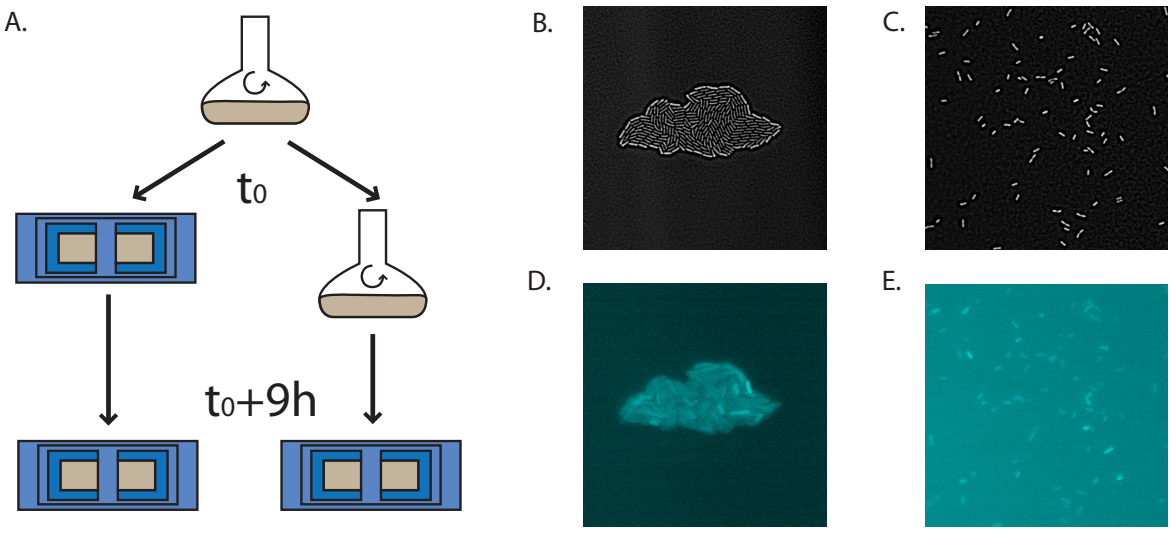

Fig. S 10: (A) Protocol for comparing solid and liquid cultures. Liquid cultures are grown for 9h before being plated on solid agar pads. Correlation images of bacteria grown in solid (B) and liquid (C) conditions. (D) and (E), Pvd fluorescence of the bacteria shown respectively in (B) and (C).

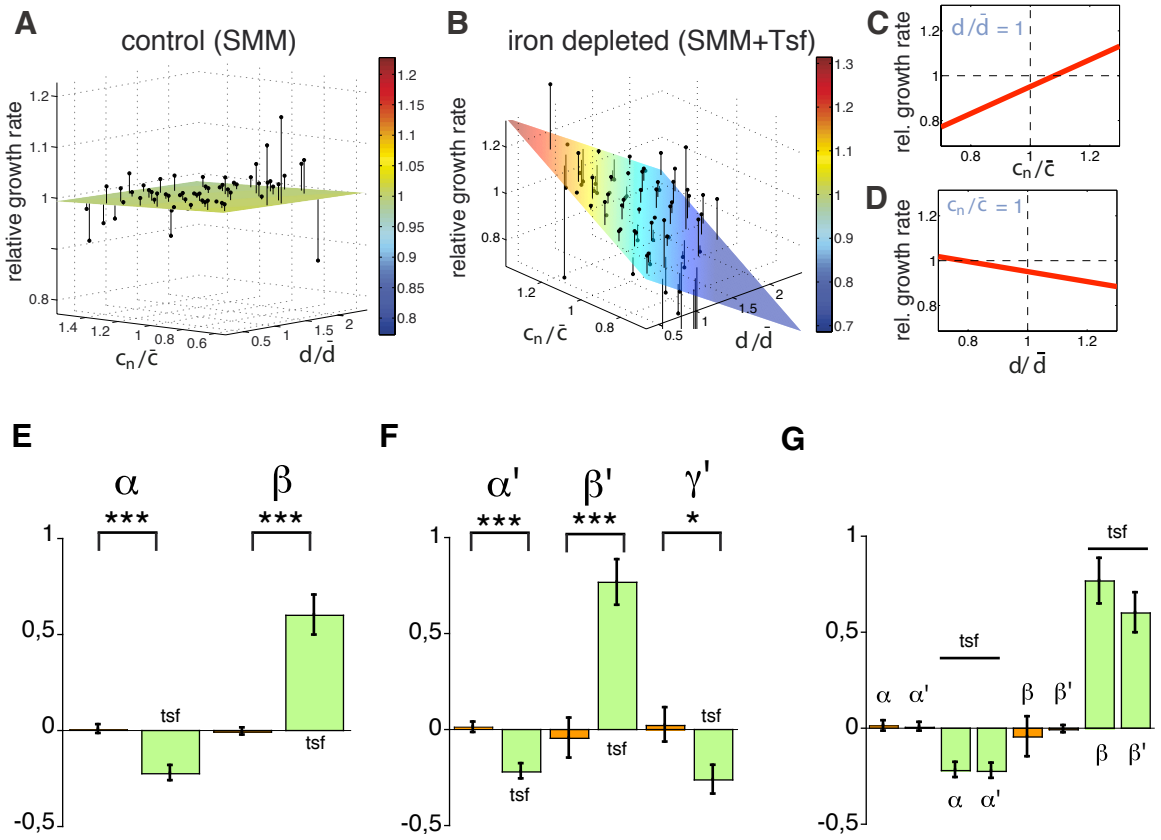

Fig. S 11: (A) and (B) The mean relative growth rate ($\nu = d(\ln L(t))/dt$, where $L(t)$ is the cell length) of cells (black points) is plotted against the distance to the colony edge (normalized by the mean radius of the colony $\bar{d}$) and the recent history of pyoverdine concentration in the cell's neighborhood c_n (normalized by $\bar{c}$). The colored planes are bivariate linear fits to the data. (A) No significant dependence is found when the level of iron is low (SMM). (B) By contrast, when iron is depleted (SMM+Tsf), the individual growth rates depend on both the position inside the colony and the pyoverdine history in the nearest neighbors. (C) and (D) Projection of the data onto the two planes. (C) The growth rate is positively correlated with the pyoverdine history in neighboring cells (slope: 0.60 ± 0.10), (D) and negatively correlated with the distance to the colony edge (slope: -0.22 ± 0.04). (E,F,G) Linear, multi-variable fits were performed separately for each microcolony growing in the two conditions: SMM = control (orange, n=10) and SMM+tsf = iron depleted (green, n=11). The error bars represent the standard errors. (E) Linear coefficients α and β were inferred from the fit $\nu/\bar{\nu} = f_0 + \alpha d/\bar{d} + \beta c_n/\bar{c}$, where $c_n(t) = \int_{-\infty}^{t} dt' e^{-\nu(t-t')} c_{\text{neigh}}(t')$ is the pyoverdine history in the nearest neighbors reflecting the fraction of iron uptake by local trafficking (Eq. 9). α quantifies the dependence of the growth rate upon distance to the edge reflecting perhaps iron depletion at the center, and β upon the history of pyoverdine in the neighborhood. (F) Linear coefficients α' and β' and γ' were inferred from the fit $\nu/\bar{\nu} = f_0 + \alpha' d/\bar{d} + \beta' c_n/\bar{c} + \gamma' c/\bar{c}$ in the same conditions. (G) Comparison of fits with two (α, β) and three variables (α', β', γ'). In Fig. 4 we only depicted the 3D representations of the fits given in (A). Error bars represent SEM, N=10.

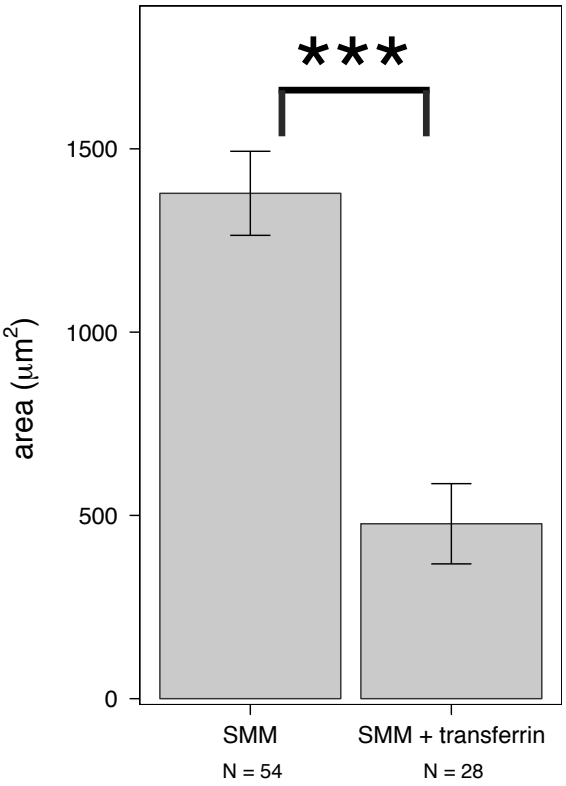

Fig. S 12: Area of the colony before the onset of double layer formation in the control medium (SMM) and in iron depleted conditions (SMM+Tsf). According to a permutation test, the area is significantly different in the two conditions ($p < 2.10^{-16}$). Error bars represent SEM, N is indicated for each condition on the bar plot.

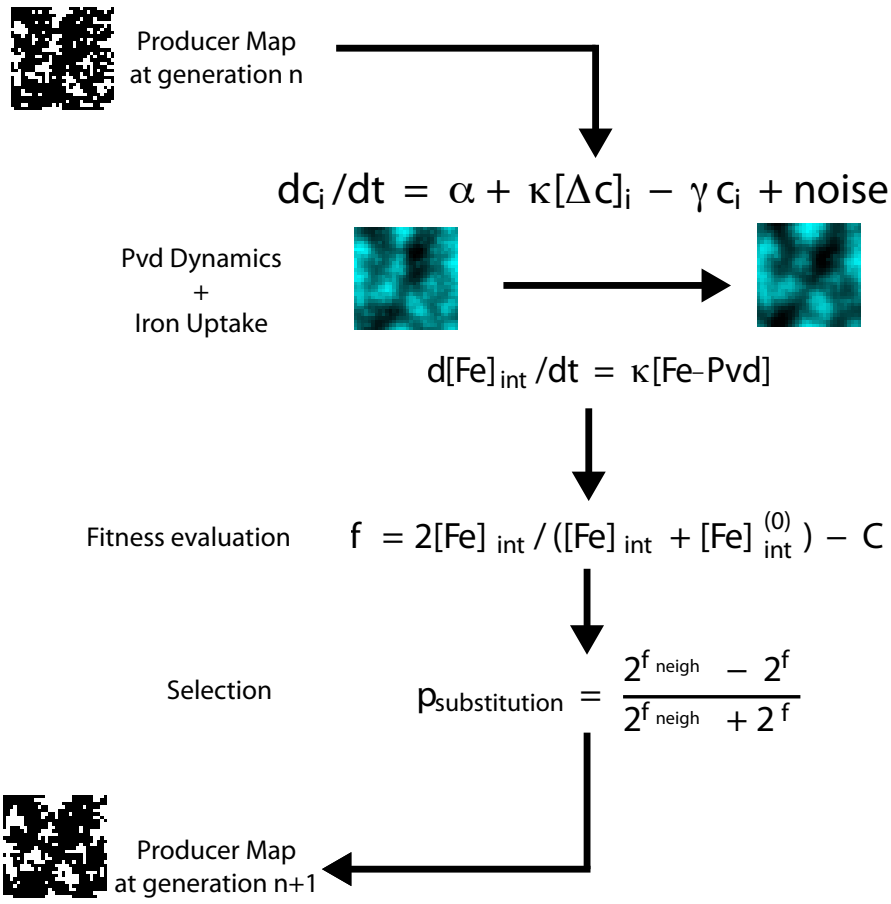

Fig. S 13: Schematic of a simulation cycle. A cycle is composed of 10 time steps. The simulation assumes synchronous divisions. During each cell cycle, pyoverdine dynamics is evaluated from the spatial model with the parameters measured in the experiments. The dynamics of iron uptake is proportional to pyoverdine uptake and iron consumption is assumed proportional to the dilution rate arising from growth. At the end of a cycle, individual fitness is evaluated as a function of iron concentration inside the cell and compared to the fitness evaluated in adjacent cells. Selection is carried out by enabling cells of highest fitness to reproduce at the expense of cells with lowest fitness. For clarity we picked up images from the simulation corresponding to an interval of 300 cycles.

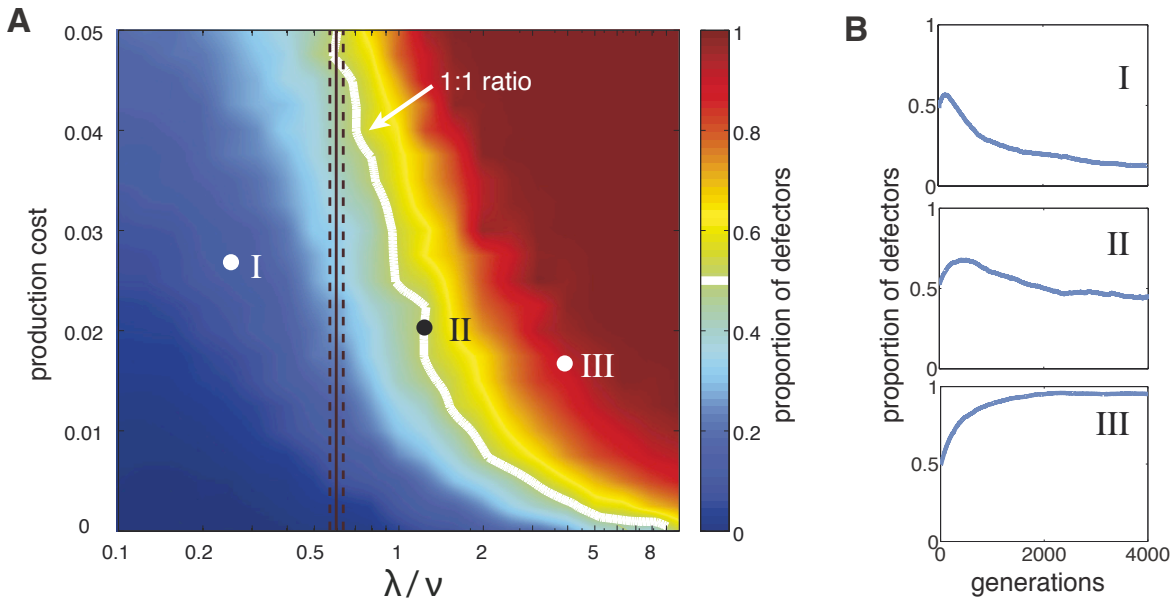

Fig. S 14: The local exchanges stabilize cooperation. (A) Phase diagram of the sustainability of cooperation in an *in silico* competition experiment between defectors and cooperators. The result of the simulation after 4,000 generations is shown as a function of the local exchange rate of pyoverdine λ, and the cost of production. Cooperators are found to dominate in a wide range of values around the measured exchange rate $\lambda/\nu \sim 0.6$. The white line depicts the initial ratio. The black line depicts the measured value of λ and the dashed lines the confidence interval. (B) Time evolution of the proportion of non-producers at the points marked in A.

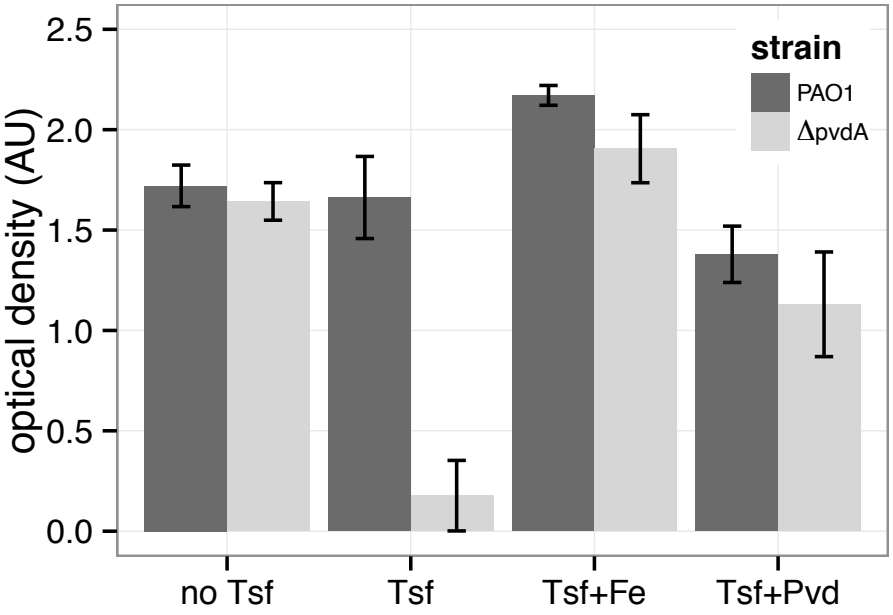

Fig. S 15: We compared the yield of a wild type strain (PAO1) with that of a production-deficient strain (ΔpvdA) in liquid culture. The culture medium was varied in order to modulate the level of iron availability: no Tsf (control medium: SMM), Tsf (iron depleted medium: SMM + 5μM Tsf), Tsf+Fe (SMM + 5μM Tsf + 100μM $FeSO_4$), Tsf+Pvd (SMM + 5μM Tsf + 30μM Pvd). For every conditions, the medium is supplemented with 20mM of $NaHCO_3$. Error bars represent SEM, N=3.

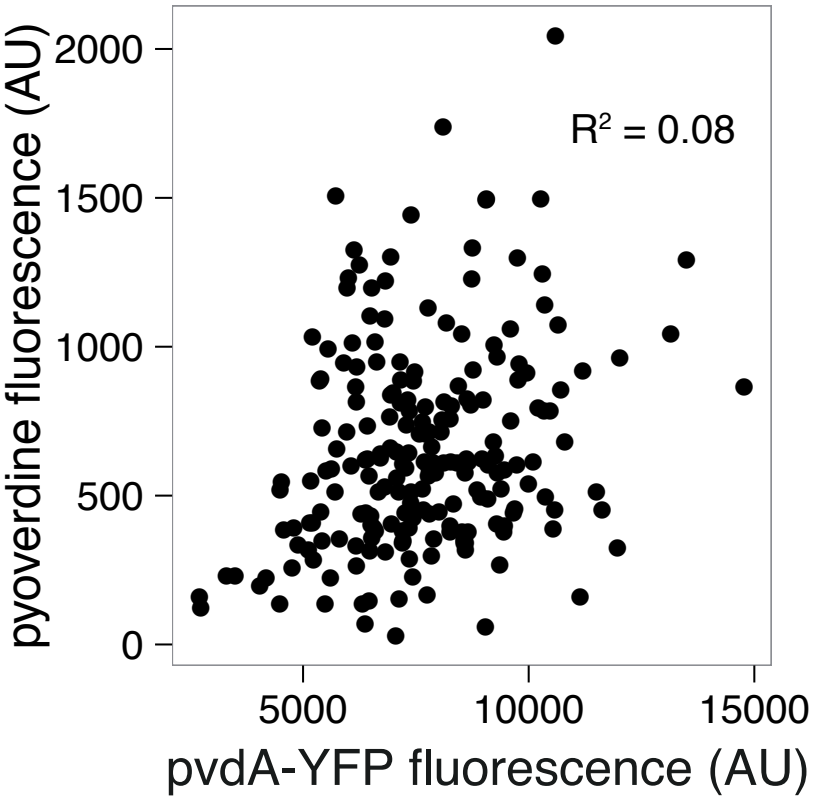

Fig. S 16: To avoid the variability due to cell-cell contacts, we measured the correlation between the level of pyoverdine and the level of production in liquid conditions . After plating bacteria on solid agar pad for observation under the microscope, we measured the signal of Pvd and YFP in individual cells of the fusion reporter strain pvdA-YFP). We estimated the percentage of the total unexplained variability by subtracting the linear contribution of production measured by fitting Pvd against PvdA-YFP and computing the remaining variability. The fraction of unexplained variability (1-R^2=92%) is the ratio of this remaining variability to the total variability.

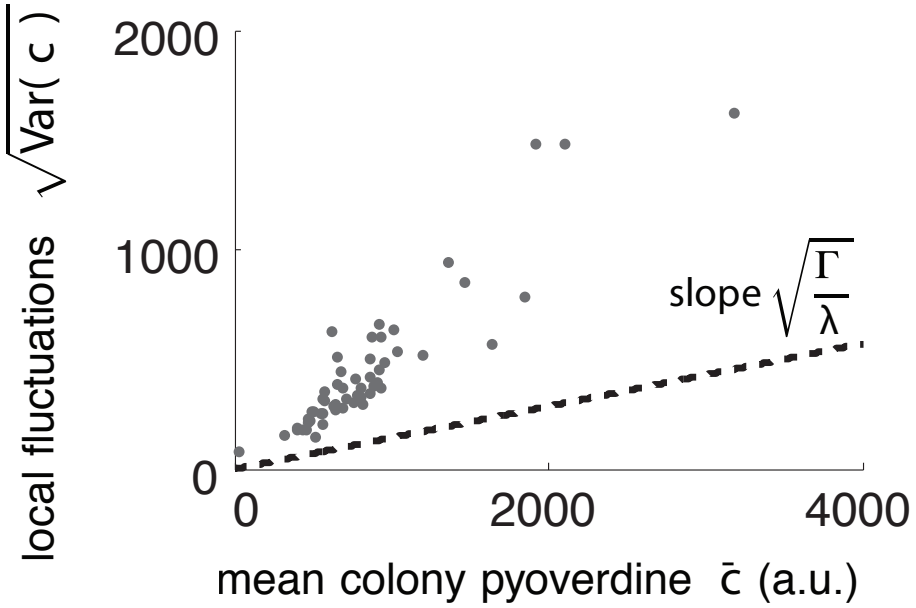

Fig. S 17: To measure the scaling of the variability in well-mixed environment, we cultivated bacteria in liquid conditions. We sampled them at different time to vary the average concentration. One point corresponds to a field of view with approximately 200 cells. In liquid conditions a linear scaling between the variability of Pvd concentration and the mean concentration is also observed. Although the model of local exchange is not relevant in this situation, the sources of the variability remain the same: noise in production, fluctuations in the number of transporters and efflux pumps. With the same sources of variability, we observed the same scaling. However since the effective exchange parameters (λ, κ, Γ, etc.) for bacteria growing in solution may be different than for bacteria growing on agar pads, we cannot use our measurements to make predictions for these different growth conditions.

References and Notes

[1] Kenney JF, Keeping ES (1951) *Mathematics of Statistics*, volume 2 (Princeton, NJ), 2 edition.

[2] Yuanhui L, Gregory S (1974) Diffusion of ions in sea water and in deep-sea sediments. *Geochimica et Cosmochimica Acta* 38:703–714.

[3] Meyer JM, Abdallah MA (1978) The fluorescent pigment of pseudomonas fluorescens: Biosynthesis, purification and physicochemical properties. *Journal of General Microbiology* 107:319 –328.

[4] Aisen P, Leibman A, Zweier J (1978) Stoichiometric and site characteristics of the binding of iron to human transferrin. *The Journal of Biological Chemistry* 253:1930–1937. PMID: 204636.

[5] Kümmerli R, Brown SP (2010) Molecular and regulatory properties of a public good shape the evolution of cooperation. *Proceedings of the National Academy of Sciences of the United States of America* 107:18921–18926. PMID: 20944065.

[6] Griffin AS, West SA, Buckling A (2004) Cooperation and competition in pathogenic bacteria. *Nature* 430:1024–1027. PMID: 15329720.

[7] Brockhurst MA, Buckling A, Racey D, Gardner A (2008) Resource supply and the evolution of public-goods cooperation in bacteria. *BMC Biology* 6:20. PMID: 18479522.

[8] Stover CK, et al. (2000) Complete genome sequence of pseudomonas aeruginosa PAO1, an opportunistic pathogen. *Nature* 406:959–964. PMID: 10984043.

[9] Yeterian E, Martin LW, Lamont IL, Schalk IJ (2009) An efflux pump is required for siderophore recycling by pseudomonas aeruginosa. *Environmental Microbiology Reports* 2:412–418.

[10] Shirley M, Lamont IL (2009) Role of TonB1 in Pyoverdine-Mediated signaling in pseudomonas aeruginosa. *Journal of Bacteriology* 191:5634 –5640.

[11] Visca P, Ciervo A, Orsi N (1994) Cloning and nucleotide sequence of the pvdA gene encoding the pyoverdin biosynthetic enzyme l-ornithine n5-oxygenase in pseudomonas aeruginosa. *Journal of Bacteriology* 176:1128 –1140.

[12] Guillon L, Mecherki ME, Altenburger S, Graumann PL, Schalk IJ (2012) High cellular organization of pyoverdine biosynthesis in pseudomonas aeruginosa: clustering of PvdA at the old cell pole. *Environmental Microbiology* 14:1982–1994.

[13] Visca P, Imperi F, Lamont IL (2007) Pyoverdine siderophores: from biogenesis to biosignificance. *Trends in Microbiology* 15:22–30.

[14] Yeterian E, et al. (2010) Synthesis of the siderophore pyoverdine in pseudomonas aeruginosa involves a periplasmic maturation. *Amino Acids* 38:1447–1459. PMID: 19787431.

[15] Ravel J, Cornelis P (2003) Genomics of pyoverdine-mediated iron uptake in pseudomonads. *Trends in microbiology* 11:195–200.

[16] Hannauer M, Yeterian E, Martin LW, Lamont IL, Schalk IJ (2010) An efflux pump is involved in secretion of newly synthesized siderophore by pseudomonas aeruginosa. *FEBS Letters* 584:4751–4755. PMID: 21035449.

[17] Schalk IJ, Lamont IL, Cobessi D (2009) Structure-function relationships in the bifunctional ferrisiderophore FpvA receptor from pseudomonas aeruginosa. *Biometals: An In-*

ternational Journal on the Role of Metal Ions in Biology, Biochemistry, and Medicine 22:671–678. PMID: 19153809.

[18] Greenwald J, et al. (2007) Real time fluorescent resonance energy transfer visualization of ferric pyoverdine uptake in pseudomonas aeruginosa. a role for ferrous iron. *The Journal of Biological Chemistry* 282:2987–2995. PMID: 17148441.

[19] Imperi F, Tiburzi F, Visca P (2009) Molecular basis of pyoverdine siderophore recycling in pseudomonas aeruginosa. *Proceedings of the National Academy of Sciences of the United States of America* 106:20440–20445. PMID: 19906986.

[20] Lamont IL, Beare PA, Ochsner U, Vasil AI, Vasil ML (2002) Siderophore-mediated signaling regulates virulence factor production in pseudomonasaeruginosa. *Proceedings of the National Academy of Sciences of the United States of America* 99:7072–7077. PMID: 11997446.

[21] Visca P, Leoni L, Wilson MJ, Lamont IL (2002) Iron transport and regulation, cell signalling and genomics: lessons from escherichia coli and pseudomonas. *Molecular Microbiology* 45:1177–1190. PMID: 12207687.